Journal of Power Sources 246 (2014) 650–658

Contents lists available at ScienceDirect

Journal of Power Sources

journal homepage: www.elsevier.com/locate/jpowsour

Review

Free air breathing proton exchange membrane fuel cell: Thermal behavior characterization near freezing temperature

Mauricio Higuita Cano [a], Sousso Kelouwani [b,*], Kodjo Agbossou [a], Yves Dubé [b]

[a] Hydrogen Research Institute and the Department of Electrical and Computer Engineering of Université du Québec à Trois-Rivières, Trois-Rivières, Québec G9A 5H7, Canada
[b] Hydrogen Research Institute and the Department of Mechanical Engineering of Université du Québec à Trois-Rivières, Trois-Rivières, Québec G9A 5H7, Canada

HIGHLIGHTS

- An investigation of the thermal behavior of a free air breathing PEMFC at low temperature.
- A model for estimating the stack internal average temperature using a minimum number of sensors.
- A brief discussion about the effect of hydrogen purge on the fuel cell voltage.

ARTICLE INFO

Article history:
Received 24 April 2013
Received in revised form
28 June 2013
Accepted 11 July 2013
Available online 29 August 2013

Keywords:
Thermal model
Hydrogen purge effect
Fuel cells temperature
Free air breathing fuel cell

ABSTRACT

A free air breathing fuel cell thermal model is developed. This proton exchange membrane fuel cell (PEMFC) has been selected as the basis for the study due to its use in automotive applications. The blowers integrated to the stack provide the required air flow for hydrogen oxidation as well as the fluid for the stack thermal regulation. Hence, their controls are a key point for keeping the system to maximum efficiency. Using well-known fuel cell electrochemistry, a dynamic thermal model near freezing temperature, which includes the stack physical parameters, is developed and validated. In addition to these parameters, only the inlet and outlet air temperatures are used to derive the model. Experimental validation with a real 1 kW free air breathing PEMFC has demonstrated that the model can reasonably track the stack internal temperature with a maximum deviation between the observed and the estimated temperatures of 5%. Therefore, the proposed method will allow the development of efficient blower management systems for PEMFC efficiency improvement.

1. Introduction

Electric vehicles are currently the best way to reduce our dependence on fossil fuels and to reduce greenhouse-gas emissions [1]. One of the main research topics is related to on-board energy storage issue. Such vehicles are mostly powered by batteries, which must have a storage capacity for autonomy comparable to gasoline vehicles. Different types of electric vehicles have been developed to meet these constraints: hybrid-electric vehicles (HEV), plugin electric vehicles (PHEVs), and fuel cell electric vehicles (FCEV) [2]. The first two vehicles have an internal-combustion engine with gasoline as fuel whilst the last one uses no fossil energy. Clearly, the FCEV has two interesting advantages (i) the low greenhouse-gas emission; (ii) high-power efficiency compared to internal-combustion engine [3,4].

The fuel cell has also a good power transient behavior. Nowadays, the proton exchange membrane fuel cell (PEMFC) is the most use hydrogen based stack technology for automotive applications. Two different types of PEMFC are being investigated for such applications: the free air breathing PEMFC and the air compressed PEMFC. The free air PEMFC is lighter and more efficient than the compressed air because it does not require a heavy and energy-intensive compressor. However, it cannot operate easily at sub-freezing temperature as the air used for the hydrogen oxidation cannot be used as temperature regulation fluid to heat the stack [5].

This paper main target is to determine a thermal behavior model of a free air breathing PEMFC which can further be used to design an optimal energy management system. So we begin

* Corresponding author.
E-mail addresses: Mauricio.Higuita.Cano@uqtr.ca (M. Higuita Cano), sousso.kelouwani@gmail.com, sousso.kelouwani@uqtr.ca (S. Kelouwani), kodjo.agbossou@uqtr.ca (K. Agbossou), yves.dube@uqtr.ca (Y. Dubé).

0378-7753/$ – see front matter © 2013 Elsevier B.V. All rights reserved.
http://dx.doi.org/10.1016/j.jpowsour.2013.07.074

Table 1
PEMFC operating conditions.

Room operating conditions	Near freezing operating conditions
Room temperature 24 °C	Outside temperature 3.5 °C
Relative humidity 17%	Relative humidity 38%
Absolute pressure of hydrogen 0.15 MPa	Absolute pressure of hydrogen 0.15 MPa
Load current 0–5 A, 0–13 A and 0–20 A	Load Current 0–5–10 A

the study by developing a transient model by analyzing the stack electrochemical behavior near the water freezing temperature and in a steady-state [6]. This electrochemical model, based on the results presented in Refs. [7–11], has been used in industry [12] as well as in the research community [11,13–15] around the world. In addition, it has been validated experimentally several times in the past. In particular, the model version in Ref. [9] has been investigated in this paper. Indeed, the model parameters are, firstly, estimated through simulation. Secondly, the model with the estimated parameters is compared with a real experimental data obtained by running a 1 kW free air breathing PEMFC. Based on this steady-state model, we derived and validated the stack transient thermal behavior. However, the hydrogen purge at the anode of each cell affects both the electrical characteristics as well as its internal temperature. In addition, a poor anode water management can increase pressure fluctuation and reduce the stack life cycle [16–19]. Indeed, as the stack is producing power, the anode water production increases, reducing the available species diffusion surface [20,21]. Hence, the purge process is mandatory to maintain good condition for reactant diffusion. So, we extend our study in order to better capture the relation between the purge process and temperature. More specifically, the work presented in the paper aims at:

- developing the transient thermal model of a free air breathing fuel cell;
- validating the obtained transient model with a real 1 kW free air breathing fuel cell;
- analyzing and discussing the effect of the hydrogen purge on the free air breathing fuel cell electric and thermal behaviors.

The rest of the paper is organized as follows. Section 2 presents the free air breathing PEMFC thermal behavior whereas the modeling approach is described in Section 3. The experimental setup and the simulation results are presented in Section 4. The purge effects and analysis are discussed in Section 5 and the conclusion is presented in Section 6.

2. Free air breathing PEMFC thermal behavior

A 1 kW free air breathing PEMFC is used for experimentation. The first step towards the development of the PEMFC thermal behavior is to observe its main parameters dynamics under different operating conditions. Two operating conditions have been selected (see Table 1).

The first operating condition is related to the room condition (normal condition) where the temperature and the air relative humidity are set constant and equal to 24 °C and 17%, respectively. During this experiment, three load current profiles are used to evaluate the real thermal behavior. The second operating condition is set in winter (outside the room) where the temperature and the air relative humidity are 3.5 °C and 38%, respectively.

2.1. Temperature sensor positions

Nine temperature sensors are positioned in the front and in the back of the fuel cell in order to capture the stack external surface thermal distribution. Five sensors labeled s_1, s_2, s_3, s_4, and s_5 are located on the front side of the stack and positioned on one main diagonal as shown in Fig. 1 (picture (a)). These sensors will permit to analyze the stack surface temperature distribution. Four additional sensors (s_6, s_7, s_8, s_9) located on one backside main diagonal are shown in Fig. 1 (picture (b)) and will allow to study the outlet air temperature distribution.

2.2. Temperature behavior

The thermal behavior of the free air breathing fuel cell is presented in Section 2.2.1 for the room condition and in Section 2.2.2 for near freezing temperature condition. The sensor distribution over the fuel cell surface allows the partition of the stack into three main zones as shown in Fig. 2(a):

- lowest zone: sensors s_1 (on the stack front side) and s_6 (on the stack backside) are used to monitor the lowest zone thermal gradient;
- middle zone: sensors s_4 (on the stack front side) and s_8 (on the stack backside) are used to monitor the middle zone thermal gradient;
- upper zone: sensors s_5 (on the stack front side) and s_9 (on the stack backside) are used to monitor the upper zone thermal gradient.

Using the infrared thermography technique, the thermal distribution over the PEMFC is shown on Fig. 2(b) for a load current of

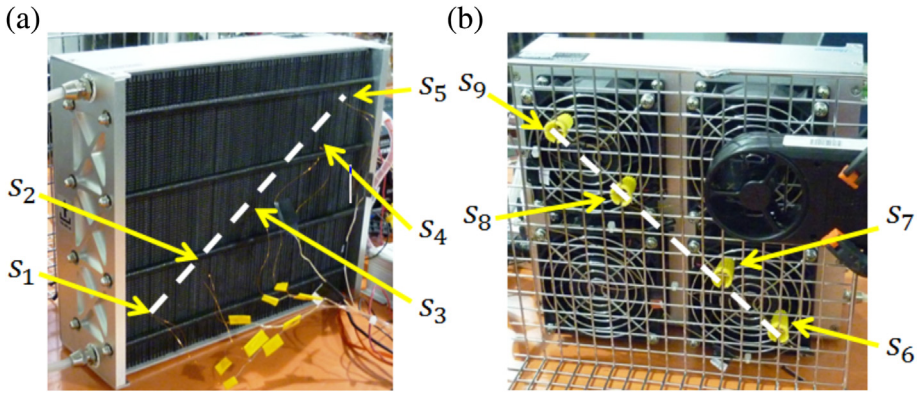

Fig. 1. Temperature sensor positions: (a) front side. (b) Backside.

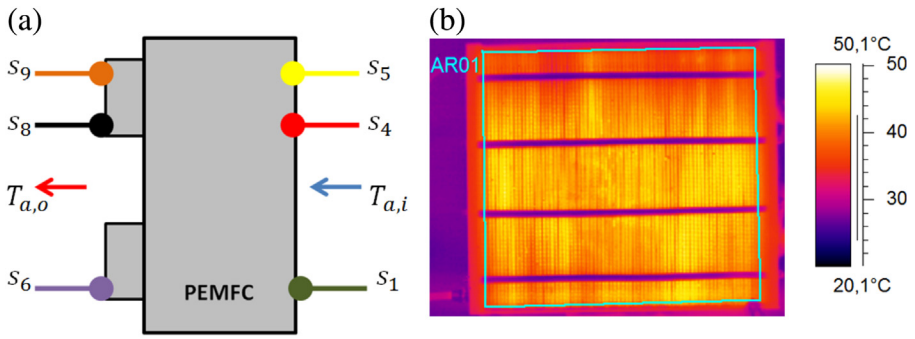

Fig. 2. Temperature behavior: (a) sensor distribution for thermal zone delimitation. (b) PEMFC front side thermography image.

20 A and a mean temperature of 47.78 °C. This thermography image reveals that the middle zone temperature is likely to be higher than the other temperature zones. In addition, the sensor's measurements of the front side of the stack (which analysis is presented in the next two sections) confirms this observation.

2.2.1. Room operating conditions

Using the three different current profiles (as defined in Table 1 of Section 2), it is desirable to analyze the stack thermal dynamics under room condition. The experimental results are shown in Fig. 3 for 5 A load current, in Fig. 4 for 13 A load current and in Fig. 5 for 20 A load current.

Three important observations can be made by analyzing these figures:

- For each current profile, the front side surface temperature values are always less than the outlet air temperature values.
- The average temperature value (s_4 and s_8) for the middle zone is always greater than the average values of the upper (s_5 and s_9) and lower zones (s_1 and s_6). This may be explained by the spatial distribution of the blowers (see Fig. 1(b)). Indeed, there is no blower in the central zone of the stack.
- In Fig. 3(c), one can observe that the s_4 measurements exhibit some fluctuations because of its position within the stack. Indeed, the thermistor sensors s_1, s_4 and s_5 are very sensitive to temperature variation and they are positioned inside the air flow channels in which the temperature may vary with the inlet flow temperature combined with the stack surface temperature.

2.2.2. Near freezing temperature operating conditions

In the same way, the experimental measurements for near freezing operating condition are shown in Fig. 6. Similar to the observations made for the room condition experimentation (see Section 2.2.1), one can see that the middle zone temperature sensor readings are always higher than the lower zone as well as the higher zone.

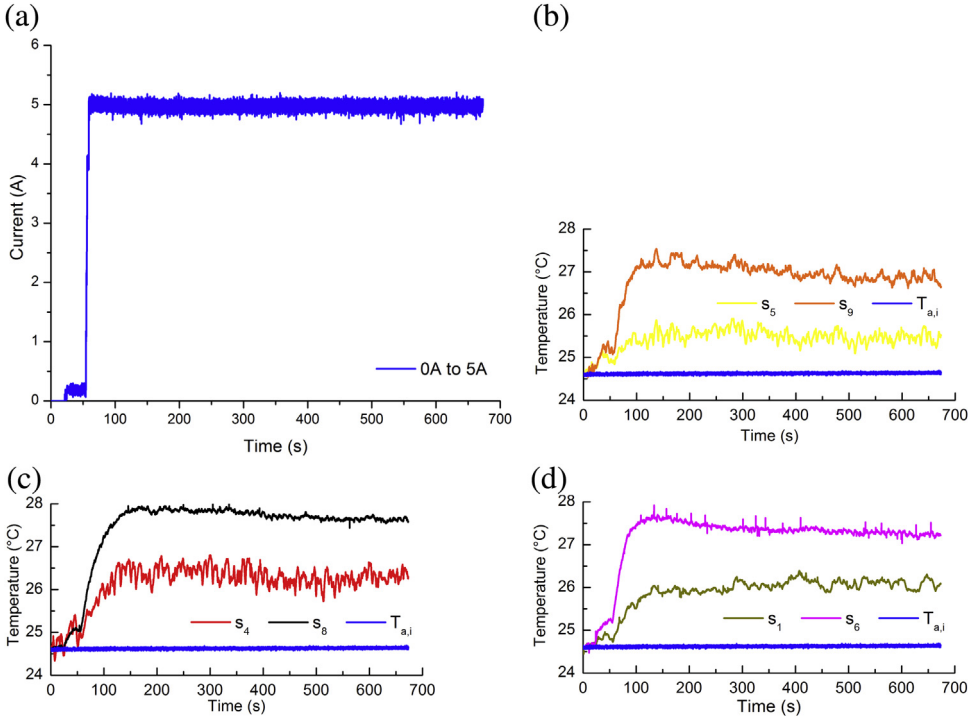

Fig. 3. Temperature profile on the PEMFC front and back sides for 5 A: (a) the load current profile; (b) upper zone temperature profiles; (c) middle zone temperature profiles; (d) lowest zone temperature profiles.

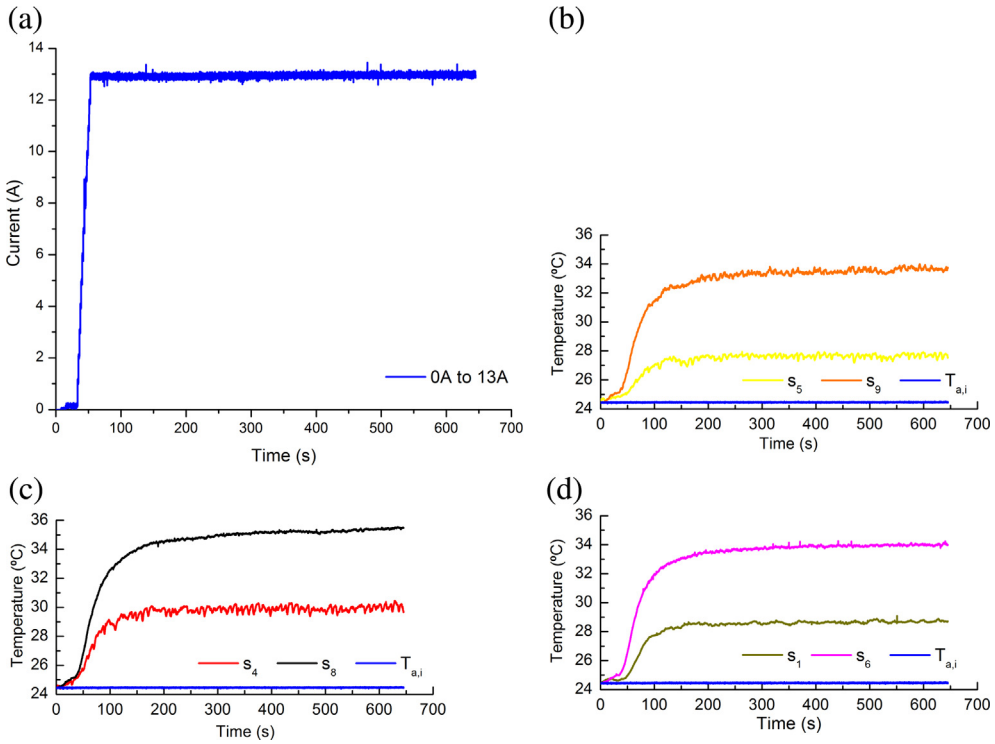

Fig. 4. Temperature profile on the PEMFC front and back sides for 13 A: (a) the load current profile; (b) upper zone temperature profiles; (c) middle zone temperature profiles; (d) lowest zone temperature profiles.

For industrial application, it is desirable to use the minimum possible number of sensors to estimate the fuel cell average temperature. As mentioned before, the middle zone is the warmer one for room and near freezing operating conditions. So, it is reasonable to select sensor s_8 as the reference sensor for the stack average temperature estimation. Recall that this sensor is positioned on the fuel cell backside. In the following section, a PEMFC stack thermal behavior will be investigated by

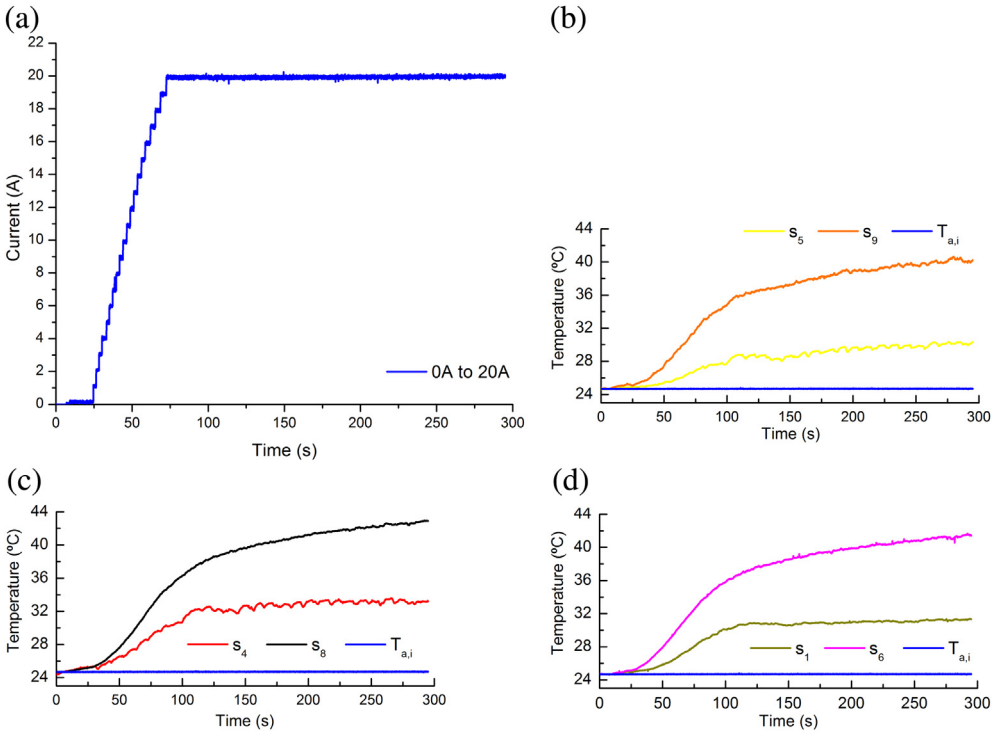

Fig. 5. Temperature profile on the PEMFC front and back sides for 20 A: (a) the load current profile; (b) upper zone temperature profiles; (c) middle zone temperature profiles; (d) lowest zone temperature profiles.

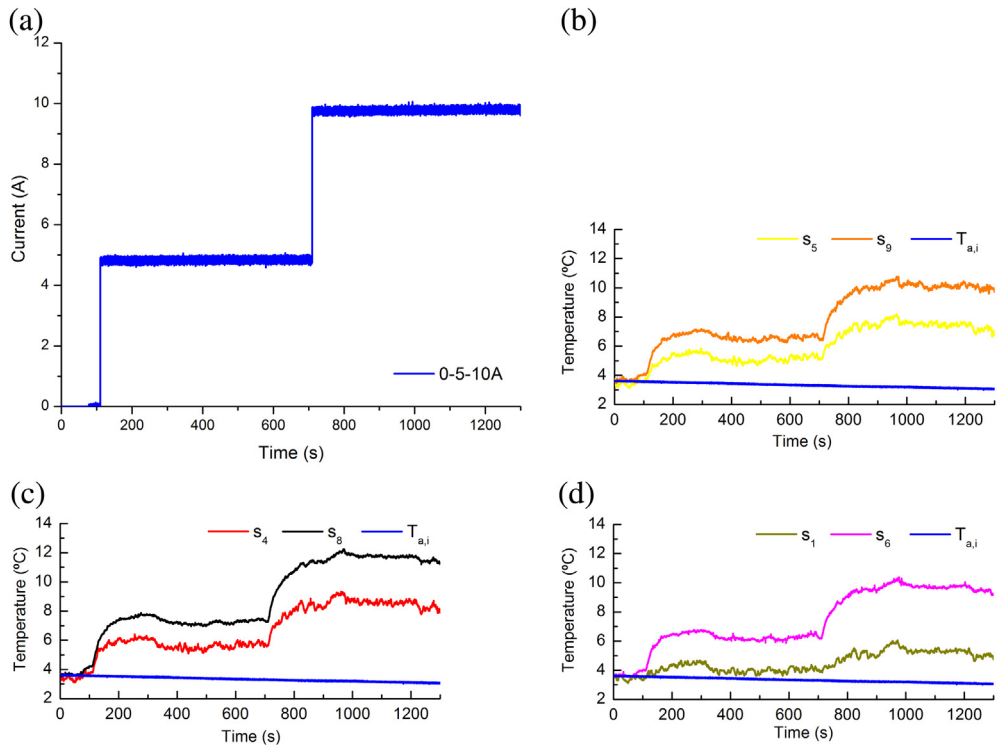

Fig. 6. Near freezing operating condition with 0–5–10 A: (a) the load current profile; (b) upper zone temperature profiles; (c) middle zone temperature profiles; (d) lowest zone temperature profiles.

considering only the s_8 data and the ambient temperature sensor.

3. Modeling approach

As mentioned before, the goal of the thermal model is to predict the mean stack temperature $\overline{T}_S$ which value will be used to improve the blower control for maximum fuel cell efficiency. The prediction should be performed using a minimum number of sensors. However, the blower speed optimal control will be addressed in a future work.

Different models have been used to describe the thermo-energetic behavior of a PEMFC. This section aims at representing the free breathing PEMFC thermal behavior, based on an electrochemical model and a heat transfer model. Therefore, the desired model is based on the following measures:

- the ambient temperature $T_{a,i}$,
- the outlet air mass flow rate $\dot{m}_{a,o}$,
- the outlet air temperature $T_{a,o}$ monitored with the sensor s_8,
- and the output net current I_S.

3.1. Free breathing PEMFC model

The thermal model used in the paper is based on the results presented in Refs. [13,15]. The exothermic reaction and the cell voltage are represented by equations (1) and (2), respectively:

$$H_2 + \frac{1}{2}O_2 \leftrightarrow H_2O \tag{1}$$

$$V_{cell} = E_{Nernst} - E_{act} - E_{ohm} - E_{con} \tag{2}$$

where E_{Nernst}, E_{act}, E_{ohm} and E_{con} represent the Nernst potential or the open-circuit voltage, the activation voltage, the ohmic voltage and the concentration voltage, respectively (see Refs. [4,9,13,22] for more details).

Thus, the power produced by a stack of N_{cell} cells when the output net current is I_S, is given by Ref. [13]:

$$P_{elec} = V_{cell} I_S N_{cell} \tag{3}$$

The Nernst potential of the fuel cell is given [23]:

$$E_{Nernst} = \frac{-\Delta G}{nF} = 1.23\ \text{V} \tag{4}$$

where

$$\Delta G = \Delta H - T\Delta S \tag{5}$$

and where n, F, ΔH, T and ΔS, represent the number of electrons per molecule, the Faraday's constant, the enthalpy of formation, the reaction temperature and the entropy, respectively.

The heat generated is represented by the following equation [13]:

$$\dot{Q}_{gen} = (E_{max} - V_{cell}) I_S N_{cell} \tag{6}$$

where E_{max} (see equation (7)) is the maximum voltage obtained using hydrogen heating value. Thus, E_{max} equals to 1.48 V or 1.23 V if hydrogen high or low heating value is used.

$$E_{max} = \frac{\Delta H}{nF} \tag{7}$$

To derive the thermal dynamics of the stack, let consider the control volume shown in Fig. 7. The parameters involved in the

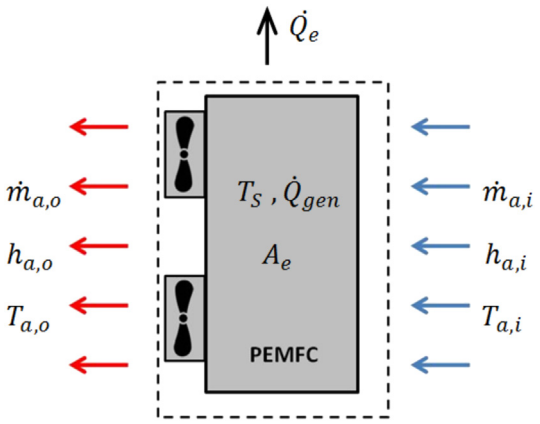

Fig. 7. Fuel cell stack heat transfer.

thermal dynamics are the transferred heat by convection between the stack and the environment (Q_e), the inlet air mass flow rate ($\dot{m}_{a,i}$), the outlet air mass flow rate ($\dot{m}_{a,o}$), the inlet heat transfer coefficient ($h_{a,i}$), the outlet heat transfer coefficient ($h_{a,o}$), the inlet air temperature ($T_{a,i}$) and the outlet air temperature ($T_{a,o}$).

The following assumptions are made:

1. the stack lumped specific heat is constant;
2. the hydrogen and the oxygen follows the ideal gas behavior;
3. the potential and kinetic energy variations are neglected;
4. the bipolar plate conduction resistance is neglected;
5. the air is flowing in rectangular channels which are positioned vertically through the bipolar plate;
6. there is no air flow leak in the stack: the inlet air flow mass rate is the same as the outlet air flow mass rate ($\dot{m}_{a,i} = \dot{m}_{a,o} = \dot{m}_a$);
7. the blower loss is neglected.

According to energy conservation rule, the dynamics of the stack thermal energy balance is represented by:

$$m_S C_p \frac{d\overline{T}_S}{dt} = \dot{Q}_{gen} + \dot{Q}_e + \dot{Q}_a \tag{8}$$

where m_S, C_p, $\overline{T}_S$, $\dot{Q}_{gen}$, $\dot{Q}_e$ and $\dot{Q}_a$ represent the stack thermal mass, the stack average specific heat capacity, the stack mean temperature, the stack heat generation rate, the stack fuel cell-environment convection heat transfer rate and the air flow heat transfer rate removed by the blowers, respectively.

The expression of $\dot{Q}_{gen}$ is given by equation (6) and equation (9) represents the stack-environment heat transfer rate [24,25].

$$\dot{Q}_e = h_{conv} A_e (\overline{T}_{a,i} - \overline{T}_S) \tag{9}$$

where h_{conv} and A_e represent the stack-environment convection heat transfer coefficient and the effective heat transfer surface, respectively.

The heat rate removed on rectangular channels running vertically through the bipolar plate can be calculated with the expression that is given by Refs. [25] and (see Fig. 8):

$$\dot{Q}_a = \dot{m}_{a,i} C_{p,a} (T_{a,i} - T_{a,o}) \tag{10}$$

where $C_{p,a}$ is the air specific heat transfer coefficient at constant pressure.

Knowing the inlet air flow velocity $v_{a,i}$, the inlet air mass flow rate $\dot{m}_{a,i}$ is given by:

$$\dot{m}_{a,i} = v_{a,i} \rho_a A_{ch} \tag{11}$$

where, ρ_a and A_{ch} represent the air density and the total rectangular channel cross section on the fuel cell front side, respectively.

Since the inlet air flow mass rate is the same as the outlet air flow mass rate ($\dot{m}_{a,i} = \dot{m}_{a,o}$), the outlet air flow velocity $v_{a,o}$ is derived using equation (12) where A_b represents the blowers cross section on the fuel cell backside.

$$v_{a,i} = \frac{v_{a,o} A_b}{A_{ch}} \tag{12}$$

The term $T_{a,o}$ in equation (10) is determined using the formula given in Ref. [24]:

$$T_{a,o} = \overline{T}_S - (\overline{T}_S - T_{a,i}) e^{-\frac{\overline{h}_{conv}\overline{A}_{conv}}{\dot{m}_{a,i} C_{pa}}} \tag{13}$$

where $\overline{h}_{conv}$ and $\overline{A}_{conv}$ represent the average heat transfer rate between the flowing air within channels and the total heat transfer surface, respectively.

$\overline{h}_{conv}$ is determined using the expression given in Ref. [24]:

$$\overline{h}_{conv} = \frac{k_a Nu_D}{D_h} \tag{14}$$

where k_a, Nu_D and D_h represent the air thermal conduction coefficient, the Nusselt number and the channel hydraulic diameter, respectively.

The Nusselt number is given by the following empirical expression [26]:

$$Nu_D = 4.36 + \frac{0.023 G_z}{1 + 0.0012 G_z} \tag{15}$$

where G_z, represent the Graetz number which value is given by Ref. [25]:

$$G_z = R_e P_r \frac{D_h}{L} \tag{16}$$

and where R_e, P_r and L represent the Reynolds number, the Prandtl number and the length of the channel, respectively.

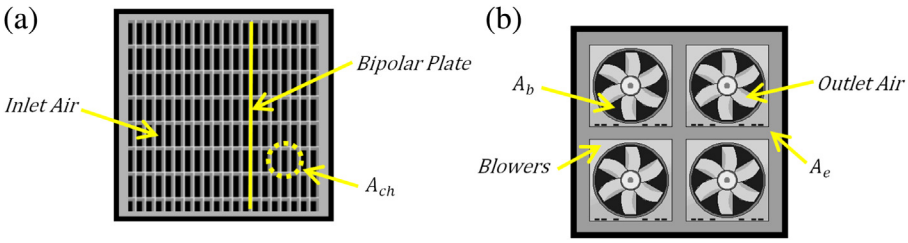

Fig. 8. Fuel cell stack technical drawing: (a) front side. (b) Backside.

In addition, the Reynolds number is computed with expression (17) [24,25]:

$$R_e = \frac{\rho_a v_{a,i} L}{\mu_a} \quad (17)$$

where μ_a represent the air viscosity. Since the obtained Reynold number ($R_e = 313$) is less than 2300, the flow is assumed to be laminar [24].

The hydraulic diameter is given by Refs. [24,25]:

$$D_h = \frac{4A_c}{P} \quad (18)$$

where A_c and P represent the air laminar flow cross sectional area and the wetted perimeter [24], respectively.

Typical values of k_a, P_r, ρ_a, μ_a and $C_{p,a}$ can be found in Ref. [27].

Substituting $\dot{Q}_{gen}$, $\dot{Q}_e$ and $\dot{Q}_a$ with their expressions (6), (9) and (10), respectively, the differential equation (8) is solved numerically.

4. Simulation and experimental results

This section aims at:

- presenting a free air breathing stack polarization curve measurements which will show the effect of near freezing temperature;
- validating the mean stack temperature model.

Before presenting the experimental results, let us introduce the test bench of the fuel cell.

4.1. Experimental setup

The stack used in our test bench is a free air breathing PEMFC provided by Horizon company (*H*1000). The stack itself, the auxiliaries as well as the data acquisition system are detailed in the following sections.

4.1.1. H1000 free air breathing fuel cell system

The test bench used during experiments is depicted in Fig. 9. The *H*1000 stack is a rated 1 kW fuel cell with 72 cells, which can deliver an output voltage between 39 V and 72 V. This stack is equipped with a controller unit (SCU) that monitors the cells temperature, the blower speed, the hydrogen purging valve operation. In addition, the controller unit can shut down the stack if the temperature exceeds 65 °C, the current exceeds 30 A or the voltage is lower than 36 V. During experiments, the outlet air velocity is measured and is kept constant to 2.3 m s^{-1}. An electronic load is connected to the stack output. The physical parameters as well as the auxiliary equipment specifications are given in Table 2.

Table 2
Test bench setup specifications.

Electrical parameters
Electronic load (Dynaload Series WCL488 Water Cooled)
External power (TENMA Model 728141 Input: 120VAC 60 Hz Output 13.8VDC Constant 6 A, 8 A)
Stack current (Hall Effect Sensor L08P100D15)
Blowers current (Hall Effect Sensor L08P100D15)
Hydrogen purge valve (On/Off 12VDC–0VDC)
Pressure
Hydrogen inlet 1 (Model 44-2260-242-017 TESCOM; 17.24 to 0.31 MPa)
Hydrogen inlet 2 (Model 44-2260-242-017 TESCOM; 0.31 to 0.05 MPa)
Flow
Hydrogen flow meter (Omega, model FMA-23 A)
Quality hydrogen (Praxair HY5.0SP 99.999%)
Air velocity meters (Velocicalc Model 9545)
Temperature
Temperature sensor (Thermistor NTC MF51E)
Temperature hydrogen sensor (Omega CLAD XL type K)
Humidity
Humidity sensor (HIH-4000-003)

4.1.2. Data acquisition system

All sensors and controllers are connected to a personal computer (PC) with LabView (version 19.0–32 bits) software installed. The main acquisition board is the National Instrument (NI) card PCIe-6323 which is also installed in the PC. Two signal conditioning modules SCB-68 from NI are also used.

4.2. Electrical characteristics

The electrical behavior of the free air breathing fuel cell is represented by the well-known polarization curves as shown in Fig. 10.

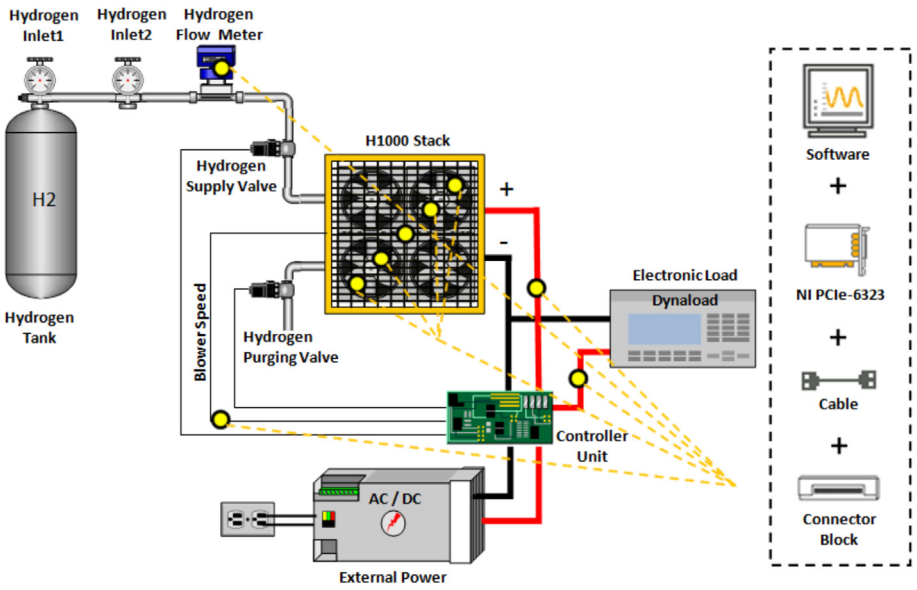

Fig. 9. Free air breathing test bench and data acquisition system.

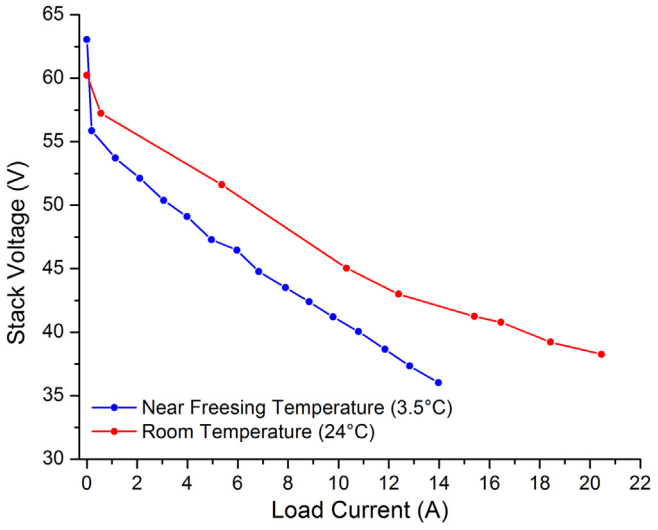

Fig. 10. PEMFC polarization curves: near freezing operating condition (blue curve) and room temperature condition (red curve). (For interpretation of the references to color in this figure legend, the reader is referred to the web version of this article.)

These curves were obtained using measurements at room condition (room temperature) and at near freezing temperature condition (outside temperature). The open-circuit voltage E_{Nernst} (load current of 0 A on Fig. 10) which is a function of the reversible voltage, is higher at near freezing temperature than at the room temperature as shown on Fig. 10. Indeed, the reversible voltage is a function of the cells' temperature [28,29]. However, the ohmic resistance increases at low temperature, limiting the available current range. At low ambient temperature $E_{\text{Nernst}} = 63.14$ V, $R_{\text{ohm}} = 1.47\ \Omega$ and RH = 38%. At room temperature, $E_{\text{Nernst}} = 60.24$ V, $R_{\text{ohm}} = 1.2\ \Omega$ and RH = 17%. Hence, we observed that the maximum currents that can be delivered by our stack before the SCU (Stack Controller Unit) shut down, are 14 A at near freezing temperature and 21 A at room temperature.

4.3. PEMFC average temperature experimental validation

The estimation of a PEMFC stack average temperature $\overline{T}_S$ proposed in this paper is based on the measurements of the ambient temperature $T_{a,i}$, the outlet air temperature $T_{a,o}$ and the air mass flow rate $\dot{m}_{a,i}$. Notice that $T_{a,o}$ is estimated using s_8. Since $\overline{T}_S$ cannot be measured directly, we provided an indirect validation as follows:

- solve numerically the differential equation (8) using the measurements of $T_{a,i}$, $\dot{m}_{a,i}$, I_S and $T_{a,o}$ to obtain $\overline{T}_S$;
- used the obtained solution $\overline{T}_S$ to compute $T_{a,o(sim)}$, the simulated value of $T_{a,o}$ by using equation (13);
- compare the simulated values $T_{a,o(sim)}$ and the sensor s_8 measurements. The estimation $\overline{T}_S$ is good enough when $T_{a,o(sim)}$ is closed to s_8 measurements.

Fig. 11 represents the experimental results of the outlet air temperature. The sub-figures (a) and (b) are related to the room operating conditions whereas the sub-figures (c) and (d) are related to the near freezing operating conditions. In sub-figures (a) and (c), the $T_{a,o(sim)}$ simulated (black curve) is compared to $T_{a,o}$ measured (red curve). The deviations between the curves of the room operating conditions and the near freezing operating conditions are represented in sub-figures (b) and (d), respectively.

The room operating conditions experiments show that the relative deviation is always lower than 4% for all tested current profiles. This result suggests that the proposed approach can estimate reasonably the stack mean temperature. On the other hand, the deviation observed at near freezing operating conditions is higher at the beginning of the experimentation but has decreased quickly with time. At the end of the experimentation, this deviation becomes lower than 5% which is an additional evidence of the capability of the proposed approach to reasonably estimate $\overline{T}_S$ at near freezing temperature.

5. Discussion

The proposed approach for a free air breathing PEMFC average temperature estimation did not consider the effect of hydrogen purge on the stack behavior. Since each PEMFC stack manufacture has its own hydrogen purge strategy, it is difficult to incorporate this functionality in the analysis. Nevertheless, we conducted several experiments in order to analyze the impact of the anodic purge (hydrogen purge) on the stack voltage as represented by equation (2).

Fig. 12 shows a typical effect of the hydrogen purge on the PEMFC under study. We can observe that a voltage drop to 0 V

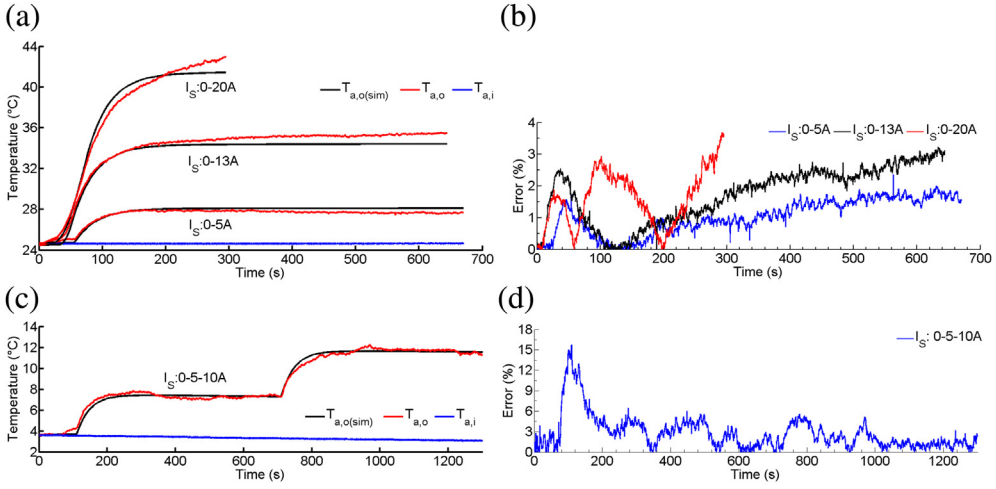

Fig. 11. Outlet air temperature validation results: (a) comparison of measured sensor $T_{a,o}$ and simulated $T_{a,o(sim)}$ at room operating conditions. (b) Deviation between $T_{a,o}$ and $T_{a,o(sim)}$ at room operating conditions. (c) Comparison of $T_{a,o}$ and $T_{a,o(sim)}$ at near freezing operating conditions. (d) Deviation between $T_{a,o}$ and $T_{a,o(sim)}$ at near freezing operating conditions.

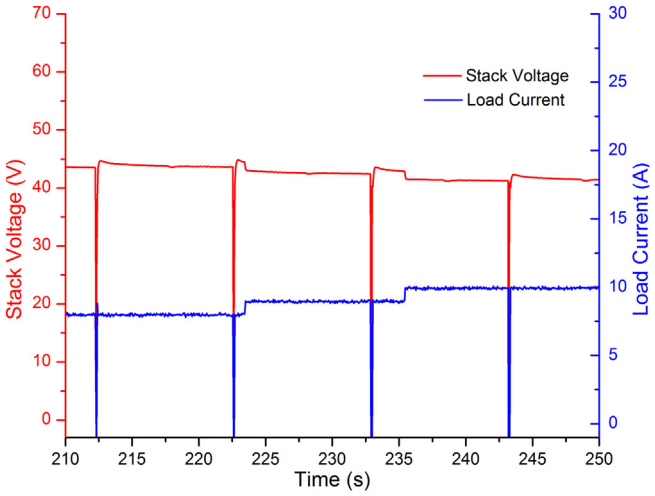

Fig. 12. Hydrogen purge effect on the PEMFC: Stack voltage (red curve). Load current (blue curve). (For interpretation of the references to color in this figure legend, the reader is referred to the web version of this article.)

occurs shortly after the purging valve is activated. During this short period of low voltage, the output current is also affected and became close to 0 A. During a long period of operation, these perturbations could affect the stack internal temperature estimation and create deviation larger than what is observed so far during this study.

6. Conclusion

A thermal model for a free air breathing PEMFC is presented. Based on well formulated and well-known hydrogen fuel cell electrochemistry, this model aims at using only the inlet air temperature (ambient temperature) and the outlet air temperature to estimate the stack internal temperature. Two different operating conditions are analyzed: room conditions (ambient temperature set to 24 °C) and near freezing operating condition (outside temperature set to 3.5 °C). The observed thermal behavior in these operating conditions has further been used to derive a thermal dynamic model with respect to the stack physical parameters. Several experimental results showed that the relative deviation between the model and experimental temperature is less than 5%. Hence, the proposed approach can reasonably track the stack internal temperature. The impact of the hydrogen purge during the stack operation has been observed but not included in the derivation of models. These purging effects on the stack average temperature will be investigated deeply in a future work.

Acknowledgment

This work was supported by H2CAN Network, “Bureau de l’efficacité et de l’innovation énergétique, Ministère des Ressources naturelles et de la Faune du Québec” and Natural Science and Engineering Research Council of Canada.

References

[1] R. Sioshansi, P. Denholm, Environmental Science & Technology 43 (2009) 1199–1204.
[2] J. Gover, A Tutorial on Hybrid Vehicles: EV, HEV, PHEV and FCEV, Kettering University, 2007.
[3] G. Jung, K. Lo, A. Su, F. Weng, C. Tu, T. Yang, S. Chan, International Journal of Hydrogen Energy 33 (2008) 2980–2985.
[4] J. Larminie, A. Dicks, Fuel Cell Systems Explained, John Wiley & Sons, 2003.
[5] H. F. C. Technologies, H-1000 Fuel Cell Stack User Manual, 2009.
[6] J. Amphlett, R. Mann, B. Peppley, P. Roberge, A. Rodrigues, Journal of Power Sources 61 (1996) 183–188.
[7] J. Amphlett, R. Baumert, R. Mann, B. Peppley, P. Roberge, T. Harris, Journal of the Electrochemical Society 142 (1995) 1–8.
[8] M. Fowler, R. Mann, J. Amphlett, B. Peppley, P. Roberge, Journal of Power Sources 106 (2002) 274–283.
[9] R. Mann, J. Amphlett, M. Hooper, H. Jensen, B. Peppley, P. Roberge, Journal of Power Sources 86 (2000) 173–180.
[10] R. Mann, J. Amphlett, B. Peppley, C. Thurgood, Journal of Power Sources 161 (2006) 768–774.
[11] F. Amrouche, B. Mahmah, M. Belhamel, H. Benmoussa, Revue des énergies renouvelables 8 (2005) 109–120.
[12] D. Xue, Z. Dong, Journal of Power Sources 76 (1998) 69–80.
[13] J. Wishart, Z. Dong, M. Secanell, Journal of Power Sources 161 (2006) 1041–1055.
[14] R. Cownden, M. Nahon, M. Rosen, International Journal of Hydrogen Energy 26 (2001) 615–623.
[15] S. Yu, D. Jung, Renewable Energy 35 (2010) 2525–2532.
[16] A. Mokmeli, S. Asghari, International Journal of Hydrogen Energy 35 (2010) 9276–9282.
[17] J. Hou, H. Yu, S. Zhang, S. Sun, H. Wang, B. Yi, P. Ming, Journal of Power Sources 162 (2006) 513–520.
[18] Y. Hou, C. Shen, Z. Yang, Y. He, Renewable Energy (2012).
[19] J. Gou, P. Pei, Y. Wang, Journal of Power Sources 162 (2006) 1104–1114.
[20] T. Pokphet, W. Khan-ngern, J. Charoensuk, in: 2010 International Conference on Electrical Engineering/Electronics Computer Telecommunications and Information Technology (ECTI-CON), IEEE, pp. 88–92.
[21] X. Yu, M. Pingwen, H. Ming, Y. Baolian, Z. Shao, Journal of Power Sources 188 (2009) 163–169.
[22] J. Lee, T. Lalk, A. Appleby, Journal of Power Sources 70 (1998) 258–268.
[23] F. Barbir, PEM Fuel Cells: Theory and Practice, Academic Press, 2005.
[24] F. Incropera, D. De Witt, T. Bergman, A. Lavine, Fundamentals of Heat and Mass Transfer, John Wiley and Sons Inc., New York, NY, 2011.
[25] J.P. Holman, J. Philip, Heat Transfer, seventh ed., McGraw-Hill, New York, 1990.
[26] H. Hausen, Darstellung des Wrmeuberganges in Rohren durch verallgemeinerte Potenzbeziehungen, VDIZ, 1943.
[27] J.e.a. Hilsenrath, Tables of Thermodynamic and Transport Properties. Reprinted by Pergamon, New York, 1960), National Bureau of Standards, 1955.
[28] H. Wang, PEM Fuel Cell Diagnostic Tools, CRC Press, 2011.
[29] K. Belmokhtar, M. Hammoudi, M.L. Doumbia, K. Agbossou, in: IEEE International Conference on Technological Advance in Electrical, Electronics and Computer Engineering (TAEECE), IEEE, 2013.